

Received 29 June 2024, accepted 15 July 2024, date of publication 19 July 2024, date of current version 29 July 2024.

Digital Object Identifier 10.1109/ACCESS.2024.3431268



## RESEARCH ARTICLE

# Research on Series Arc Fault Detection Method Based on the Combination of Load Recognition and MLP-SVM

NENGQI WU<sup>ID</sup>, MINGYI PENG<sup>ID</sup>, JIAJU WANG<sup>ID</sup>, HONGLEI WANG, QIWEI LU<sup>ID</sup>,  
MINGZHE WU<sup>ID</sup>, (Member, IEEE), HANNING ZHANG<sup>ID</sup>, AND FANFAN NI<sup>ID</sup>

School of Mechanical and Electrical Engineering, China University of Mining and Technology, Beijing 100083, China

Corresponding author: Qiwei Lu (lqw@cumtb.edu.cn)

This work was supported by the National Natural Science Foundation of China “Research on Key Technologies of Asymmetric Magnetic Coupling Resonance Radio Energy Transmission for Mining Applications” under Grant 52074305.

**ABSTRACT** In this study, a series arc fault detection method combining load recognition and multilayer perceptron-support vector machine (MLP-SVM) is proposed. The method addresses the issue of interfering loads on series arc fault detection and the lack of significant arc fault features in some loads. Initially, the eigenvalues of the line currents for single and mixed loads are extracted in the time domain, both during arc fault and normal conditions. Subsequently, load recognition is performed using a complex matrix calculation method. Then, a feature matrix and history matrix are created for each load. The history matrix is then used to compare the data in the feature matrix to detect any abnormalities in the eigenvalues of each. In the presence of any irregularity, the line current flowing through this load will be consistently gathered throughout several cycles, and processed to obtain the eigenvalues, then fed into the MLP-SVM model for training. The classification outcomes will be achieved by means of model train. The results demonstrate that the method effectively prevents misclassification of interfering loads, resulting in improved accuracy in series arc fault detection.

**INDEX TERMS** Load recognition, complex matrix, characteristic matrix, history matrix, MLP-SVM algorithm.

## I. INTRODUCTION

Arc fault is significant causative agent of electrical fires [1], [2], [3], [4]. In AC systems, there are three main types of arc fault: parallel, grounded, and series. Among these, shunt and grounding arc fault are relatively easy to detect due to the large current they produce. Conversely, series arc fault is more challenging to detect because the amplitude of the line current during a series arc fault is similar to the current amplitude under normal operating conditions. Additionally, the current waveform in series arc fault resembles that of many nonlinear loads, making detection more complex and crucial.

Previous studies [5], [6], [7], [8], [9] have utilized the physical properties of arc light, arc sound, and electromagnetic

The associate editor coordinating the review of this manuscript and approving it for publication was Mohamed Kheir<sup>ID</sup>.

radiation to detect and locate series arc fault. However, these methods are generally limited to specific switchgear cabinets and are not easily applicable to other scenarios. Consequently, some researchers have focused on detecting arc faults by extracting current or voltage eigenvalues [10], [11], [12], [13]. For instance, Literature [12] analyzed the behavior of line current under different loads and the relationship between voltage and current during series arc fault, using features such as the shoulder of the fault current waveform, pulse current, and randomness to detect arc fault. Literature [13] presents an algebraic derivative method of the line current in order to detect the presence of series arcs in an AC or DC electrical installation. However, solely analyzing current or voltage eigenvalues can lead to susceptibility to interference from other loads.

With the advancement of artificial intelligence, machine learning algorithms have shown promising performance in

fault detection across various fields [14], [15], [16], [17]. The use of machine learning for series arc fault detection is an emerging area of research. For example, Literature [18] proposed a feature selection method combining Euclidean distance, classifier criterion, max-relevance min-redundancy and clustering index is proposed, and a variational Bayesian optimization-based stochastic configuration network (VBS-CN) algorithm for series arc fault detection. Literature [19] combined wavelet transform and singular value decomposition (SVD) to extract characteristics of localized discharge signals. Literature [20] developed a tandem arc fault detection method based on category identification and artificial neural networks after analyzing the current characteristics of arc fault under different loads. Literature [21] proposed a low voltage AC series arc fault localization method based on a radial basis function (RBF) neural network. These methods, however, often require extensive data training and involve complex algorithms, which can limit their practicality.

When a series arc fault occurs, the line current waveform can resemble the current waveform of some loads during normal operation, potentially leading to misjudgments. Additionally, series arc fault impact the line current differently depending on the type of load. If the load type is known in advance during series arc fault detection, the accuracy of detecting arc fault can be significantly improved. Therefore, in recent years, several academics have suggested incorporating load identification prior to series arc fault detection in order to mitigate the impact of specific disruptive loads. This approach has the potential to significantly enhance the accuracy of the algorithm, making it more applicable and practical [20], [22], [23]. Literature [20] categorizes loads into three types: resistive, resistive-inductive, and rectifying circuits with capacitive filters. It utilizes neural networks for series arc fault detection, and optimizes the initial weights and thresholds of these neural networks using genetic algorithms. Reference [22] presented a methodology that utilized a combined principal component analysis and support vector machine (PCA-SVM) model to identify loads and detect series arcs. Based on the fact that different types of load circuits exhibit distinct current characteristics, the literature [23] trained a Learning Vector Quantization Neural Network (LVQ-NN) and developed a Particle Swarm Optimization Support Vector Machine (PSO-SVM) algorithm to detect arc fault. However, Literature [20] fails to identify specific loads, increasing the complexity of the detection model. Furthermore, Literature [22], [23] only focuses on single load identification, which introduces certain limitations. To address the aforementioned issues, this work provides a series arc fault detection approach that combines load recognition and the MLP-SVM model. In the load identification link, the formula method is first used to solve the complex matrix equation to determine whether the load is a single load and reflect its type; conversely, if the formula method is used to determine the load as a composite load, the combination of the formula method and the exhaustive method is used to determine the individual components in the mixed load

to achieve effective identification of the mixed load. The load identification realized by these two methods avoids the influence of the wide variety of load types on arc detection. Then the MLP-SVM model is utilized to detect series arc fault, which reduces the difficulty of series arc fault detection and also achieves higher detection accuracy.

## II. EXPERIMENTAL PLATFORM CONSTRUCTION

Figure 1 displays the schematic diagram of an AC series arc fault experiment, which consists of an AC power source, an arc generating device, a signal acquisition device, and a load. This study presents the construction of a series arc fault test platform, which adheres to the relevant requirements both domestically and internationally [24], [25], [26]. The platform is depicted in Figure 2.

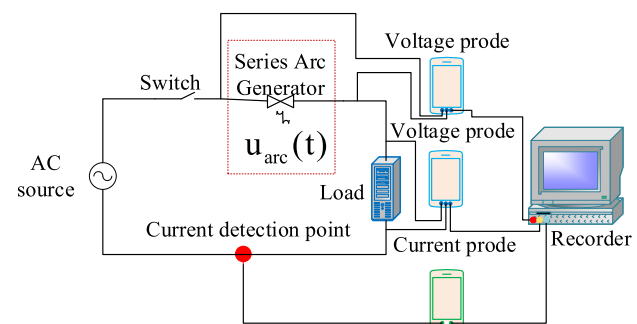


**FIGURE 1.** Experimental schematic.

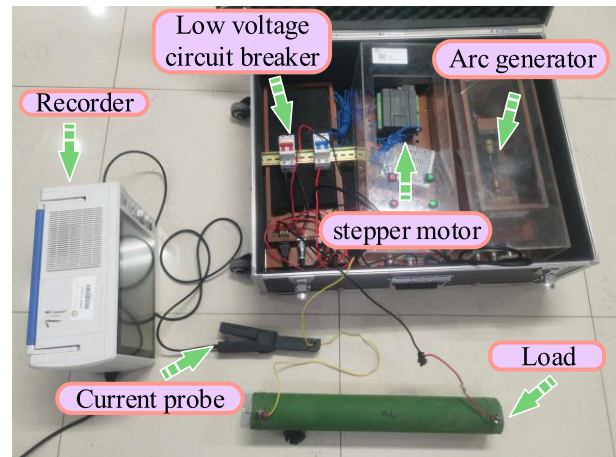


**FIGURE 2.** Arc fault experiment platform.

The fault arc generator in this scenario comprises a stationary electrode, a mobile electrode, and a stepper motor for precisely modifying the gap between the electrodes. The stepper motor is employed to precisely position the moveable slider in order to achieve complete contact between the two electrodes. After that, the circuit is powered, and the distance between the two electrodes is incrementally modified using the adjustable slider. An electric arc is formed when the distance between the two electrodes hits a specific threshold.

**TABLE 1.** Load parameter information table.

Load Serial Number	Load Name	Power/W	Load Type
1	Electric fan	60	Inductive load
2	Incandescent lamp	300	Resistive load
3	Dust catcher	1100	Resistor-Capacitor Filter Load
4	Evaporative cooling fan	65	Inductive load
5	Monitor	18	Resistor-Capacitor Filter Load
6	Electric fan + Monitor	60+18	Two mixed loads
7	Evaporative cooling fan + Monitor	65+18	Two mixed loads
8	Electric fan + Evaporative cooling fan + Monitor	60+65+18	Three mixed loads

The experiment collected data such as the waveform of arc voltage, load terminal voltage, and line current. The sampling frequency was 50kHz, meaning that 1,000 points were recorded per cycle at the industrial frequency of 50Hz. Table 1 displays the loads employed in this experiment for the purpose of gathering information. Figure 3 displays the waveforms of the current flowing through the load in two scenarios: normal conditions and when an arc fault occurs.

### III. BASIC PRINCIPLE AND TESTING PROCESS

#### A. PRINCIPLES OF MULTILAYER PERCEPTRON ALGORITHM

The multilayer perceptron (MLP) is a type of neural network that consists of multiple layers, including input, hidden, and output layers, arranged in a hierarchical structure. The neurons in each layer are interconnected through weights and undergo a nonlinear transformation through an activation function. MLP is capable of approximating any continuous function, making it suitable for solving nonlinear regression problems. The objective of training the MLP is to optimize the hyperparameters by adjusting the weights and bias values in order to minimize the loss function [27], [28]. Figure 4 displays the block diagram illustrating the structure. The input variables are denoted as  $x_1$ ,  $x_j$ , and  $x_M$ . The hidden layer consists of the neuron models  $\theta_1$ ,  $\theta_i$ , and  $\theta_q$ . The output layer contains the neurons  $\alpha_1$ ,  $\alpha_k$  and  $\alpha_L$ . The output variables are represented by  $O_1$ ,  $O_k$ , and  $O_L$ . The weight between  $x_M$  in the input layer and neuron  $\theta_q$  in the hidden layer is represented by the variable  $w_{qM}$ . Similarly, the weight between neuron  $\theta_q$  in the hidden layer and neuron  $\alpha_L$  in the output layer is represented by the variable  $w_{Lq}$ .

#### B. PRINCIPLES OF SUPPORT VECTOR MACHINE ALGORITHM

Support Vector Machine (SVM) algorithm is a binary classification model, which is to find a hyperplane in the feature

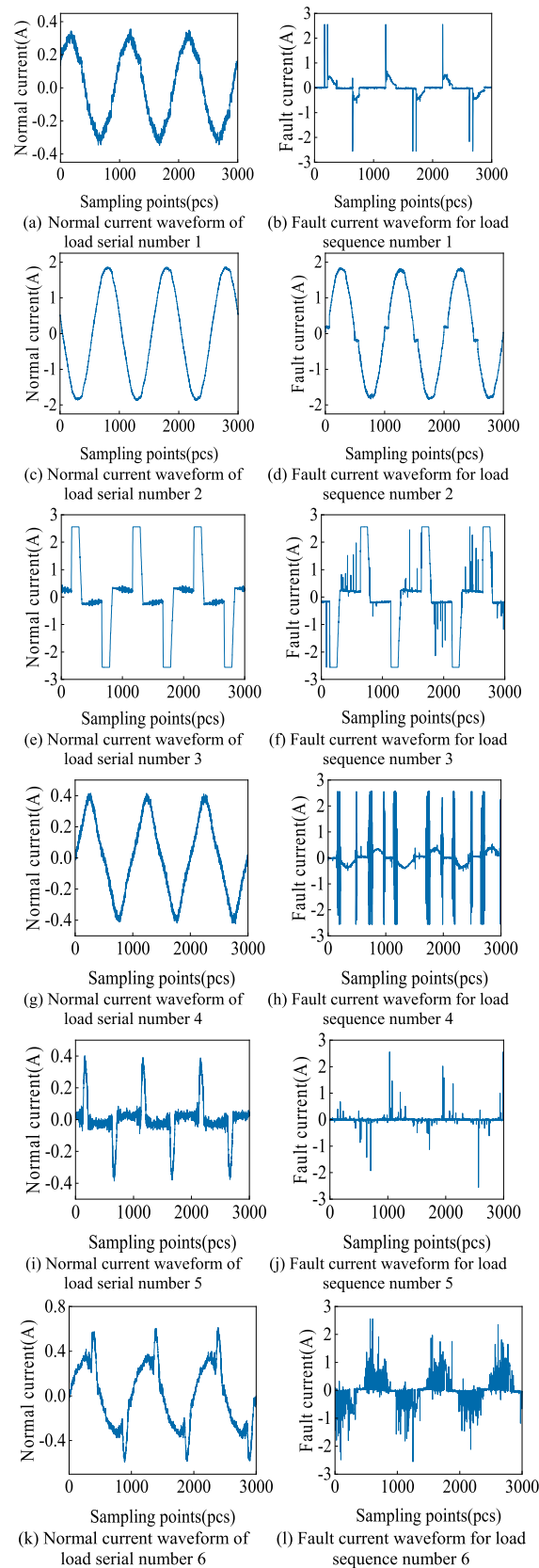


**FIGURE 3.** Line current waveforms for loads under normal conditions and under arcing fault conditions.

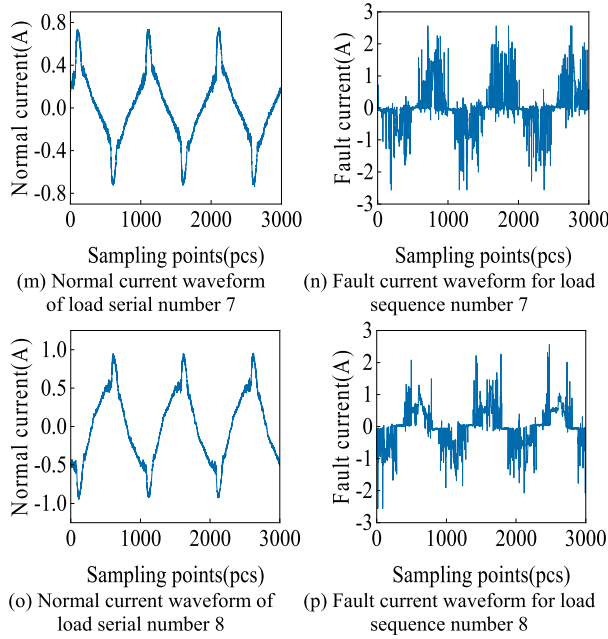


**FIGURE 3. (Continued.)** Line current waveforms for loads under normal conditions and under arcing fault conditions.

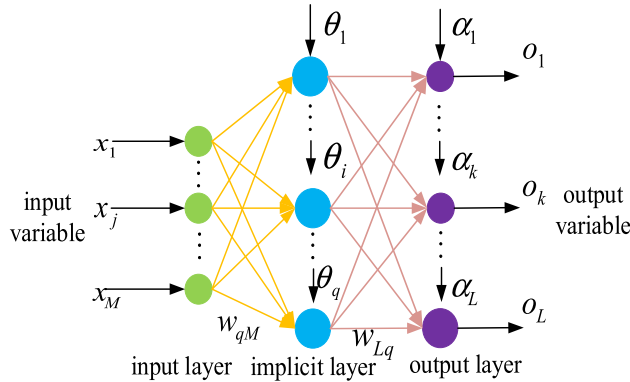


**FIGURE 4.** Schematic diagram of MLP algorithm.

space that can separate samples of different classes and maximize the distance from the nearest sample point to the hyperplane [29], [30], [31]. For example, for a given set of training samples as  $M$ ,  $a_i$  is the  $i$ th feature vector and  $b_i$  is the class labeling,  $w$  is the plane normal vector and  $y$  is the intercept. it can be partitioned by a hyperplane as represented in equation (1).

$$w^M a + y = 0 \quad (1)$$

The minimum distance between the training sample points under two different classifications is defined as equation (2).

$$b = \min_{(a|b=1)} \frac{w^M a + y}{|w|} - \max_{(a|b=-1)} \frac{w^M a + y}{|w|} = \frac{2}{|w|} \quad (2)$$

Thus, as in equation (3), the SVM algorithm models the maximum segmentation hyperplane problem by optimizing

the following constraints.

$$\max_{w,y} \frac{1}{2} \|w\|^2 \text{ s.t. } b_i (w^M a_i + y) \geq 1, \quad i = 1, 2, 3, \dots, m \quad (3)$$

For convex quadratic programming formulations containing inequality constraints, the optimal parameters  $w$  and  $y$  can be solved using the Lagrange multiplier method and the pairwise algorithm.

### C. MLP-SVM COMBINED MODELING PRINCIPLES

Integrated learning is an educational approach that combines many less effective learners by assigning weights to the samples and learners in order to achieve a more powerful learner with exceptional generalization abilities. This approach necessitates that individual learners possess a specific degree of precision as well as a specific degree of diversity. The fundamental concept is to employ diverse sampling or preprocessing techniques on the training data in order to create several base learners and merge them into a unified model, hence enhancing the overall predictive accuracy and generalization capability.

Hence, this article aims to integrate the MLP method with the SVM algorithm to create the MLP-SVM combined model. Initially, the model is trained using a set of hyperparameters selected from a given space. The training is performed on the training set, while the validation set is used for testing. This process is repeated iteratively within the hyperparameter selection space to identify the best model with optimal hyperparameters. The accuracy of the validation set on the model is recorded throughout this process. Next, the accuracy of various models on the validation set is evaluated. If there is a significant difference in accuracy, the model with the higher accuracy is chosen as the final model. If the difference in accuracy is less than a certain threshold  $\theta$ , the two models are combined using weights, and the final prediction is calculated as the weighted sum of the predicted values from both models. Figure 5 displays the diagram of the integrated model.

### D. TESTING PROCESS

This paper first identifies the loads using a complex matrix. It then establishes a feature matrix and a history matrix for each load. The loads are monitored through the history matrix, and the monitoring values in the history matrix are compared with the feature matrix for assessment. If there is an eigenvalue in the load's monitoring value that exceeds the threshold range, the line current data within 1 second is collected continuously as a test set for the load. This test set is then inputted into the MLP-SVM model for detection, and the classification results are obtained after training the model. As per the literature standards [25], [26], if there are 14 or more half-cycle arc faults within 1 second, the arc fault detector must promptly emit an alarm signal. Hence, if there are 14 anomalous sample points in the classification outcome,

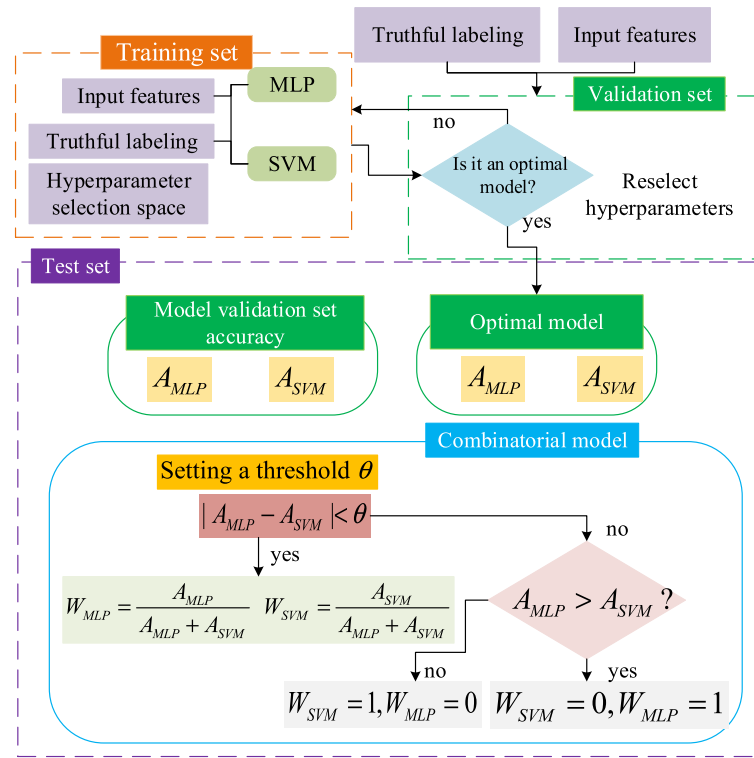


**FIGURE 5.** Schematic diagram of the combined MLP-SVM model.

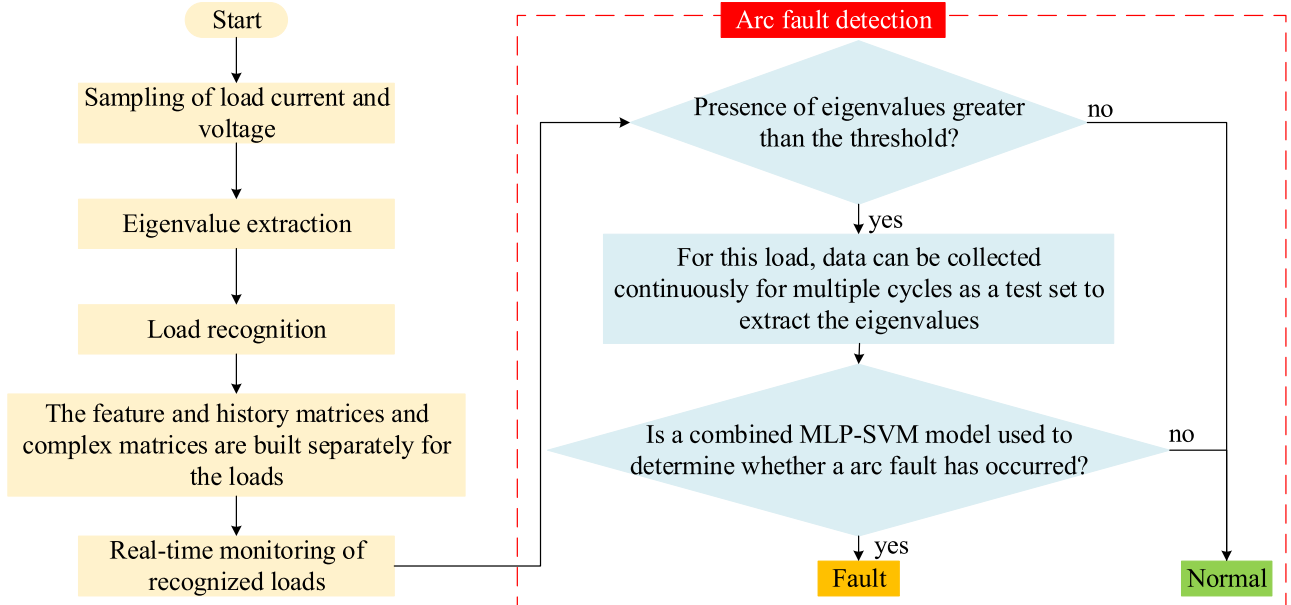


**FIGURE 6.** Flowchart of the combined model.

it is determined that a fault in the form of an arc has transpired in the line. Figure 6 displays the flow chart for detection.

#### IV. LOAD RECOGNITION

##### A. THE NEED FOR LOAD RECOGNITION

To mitigate the impact of specific interfering loads on arc detection, incorporating load recognition prior to arc detec-

tion might enhance the precision of future arc fault detection methods. The current data of the line under normal operation and during the occurrence of a series fault arcing state are gathered by conducting experiments with the loads listed in Table 1. Subsequently, both the regular functioning of each load and the instances of arc fault are categorized. The loads are categorized and labeled according to their load serial

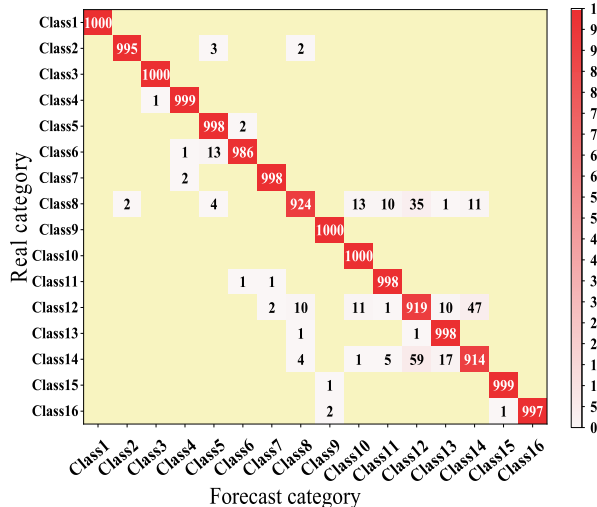


**FIGURE 7.** Load categorization confusion matrix diagram.

numbers in Table 1. Load serial number 1 is categorized as category 1, representing normal operation. Category 2 represents an arcing fault happening. Load serial number 2 is categorized as category 3, representing normal operation, and so on. The loads are classified based on the MLP-SVM model, and the accuracy of the predicted labels is assessed using the confusion matrix. The confusion matrix in this scenario represents the connection between the predicted and actual labels of the samples, illustrating the model's binary classification difficulty.

The confusion matrix was utilized to compare the actual categories of the loads with the categories in the post-categorization. The outcomes of the experiment are depicted in Figure 7. The confusion matrix in Figure 7 represents the true categorization of the samples in each row, and the expected categorization of the samples in each column.

Figure 7 illustrates a phenomenon where certain loads in the normal operation and arc fault categories are incorrectly classified into different categories. For example, a small amount of class 8 was categorized into class 10, class 11, and class 14, and most were categorized into class 12. Class 12 is mostly categorized into class 14. The presence of power electronic switches in these loads, along with the flat shoulder phenomenon, current waveform shape, and other characteristics, complicates the classification process and leads to the phenomenon of categorization crossover. This makes it difficult to detect arc faults and increases the likelihood of misjudging line fault arcs in the absence of load categorization. Thus, this article aims to simplify the task of identifying all loads by accurately recognizing the loads and arc fault detection on various loads.

## B. FEATURE VALUE SELECTION FOR LOAD RECOGNITION

Kirchhoff's current law states that the total current flowing through a load in a circuit is equal to the sum of the currents flowing through each branch of the circuit. The Fourier

transform has the purpose of breaking down the waveform of a signal in the time domain into a combination of several sinusoids with varying frequencies. Hence, in this study, the fast fourier transform (FFT) technique is employed to convert the normal operating current of each load. By performing calculations, the real and imaginary components of the fundamental current amplitude and each harmonic amplitude are determined. These values serve as the indicators for load identification [32]. The outcome of the FFT transformation aligns with the principle of superposition, specifically.

$$(I_{a1} + jI_{b1}) + (I_{a2} + jI_{b2}) + \dots + (I_{an} + jI_{bn}) = I_{SUM} + jI_{SUM} \quad (4)$$

In Eq. (4),  $I_{a1}$  and  $jI_{b1}$  are the real and imaginary parts, respectively, of the A1 load after FFT transformation of the current signal,  $I_{a2}$  and  $jI_{b2}$  are the real and imaginary parts, respectively, of the A2 load after FFT transformation, and so on.

Therefore, the process of load identification can be transformed into a matrix form as shown in equation (5),

$$AX = B \quad (5)$$

In equation (5),

$$X^T = (X_1, X_2, X_3, \dots, X_n)$$

$$B^T = (I_1 + jI_1, I_3 + jI_3, I_5 + jI_5, I_7 + jI_7, I_9 + jI_9)$$

$$A = \begin{pmatrix} a_1 + ja_1 & b_1 + jb_1 & c_1 + jc_1 & \dots & n_1 + jn_1 \\ a_3 + ja_3 & b_3 + jb_3 & c_3 + jc_3 & \dots & n_3 + jn_3 \\ a_5 + ja_5 & b_5 + jb_5 & c_5 + jc_5 & \dots & n_5 + jn_5 \\ a_7 + ja_7 & b_7 + jb_7 & c_7 + jc_7 & \dots & n_7 + jn_7 \\ a_9 + ja_9 & b_9 + jb_9 & c_9 + jc_9 & \dots & n_9 + jn_9 \end{pmatrix}$$

where  $a_1 + ja_1$  denotes the real and imaginary parts of the fundamental of the current of load a,  $a_3 + ja_3$  denotes the real and imaginary parts of the third harmonic of the current of load a, and so on.  $X$  is the required solution and  $B$  is a matrix of order  $5^*1$ .

## C. METHOD OF LOAD RECOGNITION AND INSPECTION PROCESS

This study combines the formula approach with the exhaustive method proposed in the literature [32] to improve load identification detection. By doing so, it decreases misclassification caused by the formula method and enhances the detection rate of the exhaustive method. The process of using the formulaic approach to solve Equation (5) and obtain the solution for  $X$  is demonstrated in Equation (6).

$$X = (A'A)^{-1}A'B \quad (6)$$

The solution value of the circuit is directly proportional to the number of loads connected to it. The exhaustive enumeration method involves progressively traversing all the data in a dataset where all the answers are present in order to identify the one that satisfies the user's criteria. Setting the number of standard individual loads in the circuit to five. To completely deplete the circuit, a single load is referred to as a one-time

**TABLE 2.** Real and imaginary parts of 8 loads.

Load Serial Number	Fundamental		3rd harmonic		5th harmonic		7th harmonic		9th harmonic	
	Real part	imaginary part	Real part	imaginary part	Real part	imaginary part	Real part	imaginary part	Real part	imaginary part
1	0.19889	-0.23123	0.0044798	-0.0047087	0.00979234	-0.00501099	0.00599232	-0.0003036	0.00395606	-0.000591
2	1.853097	-0.204545	0.0119708	0.000837	0.01999013	0.000628215	0.0149926	0.00047116	0.00495659	0.0033811
3	0.813826	1.1842693	-0.9341207	0.5156623	-0.4666091	-0.0940849	-0.0231046	-0.0064944	-0.1477764	-0.2102645
4	0.330347	0.088516	0.02587524	-0.0368167	0.00366265	-0.00160779	-0.00040557	-0.0019585	0.00073016	-0.0006833
5	0.083154	-0.025582	-0.0061198	-0.0777596	-0.0565729	-0.0377294	0.0234005	-0.0508765	-0.031987	-0.0240168
6	0.29939	-0.246798	-0.0017592	-0.0839816	-0.048666	-0.0415647	0.03063258	-0.0515911	-0.0302228	-0.0246491
7	0.408778	0.058905	0.01834633	-0.11454	-0.0565069	-0.0378281	0.022941639	-0.0532699	-0.0348605	-0.0234253
8	0.607821	-0.173142	0.02433503	-0.1164852	-0.0472854	-0.040101	0.02974989	-0.0566652	-0.0261093	-0.0276098

**TABLE 3.** Formula load recognition results.

Load Serial Number	a	b	c	d	e
1	1.0+9.632e-12i	-3.733e-12 +8.491e-13i	7.461e-14 +4.364e-14i	-1.549e-12+4.968e-12i	4.326e-13 -1.899e-13i
2	5.103e-11 +6.123e-11i	0.9999-6.1285e-12i	9.221e-13 +1.3706e-13	-6.941e-12 +2.004e-11i	8.0507e-13 -2.076e-12i
3	-9.0201e-12-5.459e-11i	-1.494e-12-2.8436e-12i	1.0 -8.137e-13i	4.3807e-12 -3.004e-11i	-4.826e-12 +1.192e-12i
4	-9.021e-12 -1.481e-12i	-1.414e-12 -1.296e-12i	-8.946e-14 -6.295e-14i	0.99999 -3.471e-12i	-2.514e-13 +7.637e-13i
5	3.8703e-12+1.478e-12i	-1.548e-12+ 2.543e-13i	5.242e-14 -1.424e-14i	2.757e-13 +9.204e-13i	0.99999 -1.487e-13i
6	0.88745 +0.081082i	-0.000181 +0.01796i	-0.0023 -0.006i	-0.02066 -0.17288i	1.0403 +0.025i
7	-1.26637 -0.69009i	0.22643 +0.05847i	-0.0178 -0.0134i	0.76647 -0.5327i	1.01732 +0.0903i
8	3.5999 +4.195i	-0.70479-0.53893i	0.04771+0.043i	1.2066 +1.6156i	1.2174 -0.25795i

$$X = \begin{pmatrix} 1 \\ 0 \\ 0 \\ 0 \\ 0 \end{pmatrix} X = \begin{pmatrix} 0 \\ 1 \\ 0 \\ 0 \\ 0 \end{pmatrix} X = \begin{pmatrix} 0 \\ 0 \\ 1 \\ 0 \\ 0 \end{pmatrix} X = \begin{pmatrix} 0 \\ 0 \\ 0 \\ 1 \\ 0 \end{pmatrix} X = \begin{pmatrix} 0 \\ 0 \\ 0 \\ 0 \\ 1 \end{pmatrix}$$

**FIGURE 8.** Exhaustive array.

exhaustion, as seen in Figure 8. Therefore, at this juncture, it is necessary to exhaust the circuit 5 times. To calculate mixed loads, add the real and imaginary components of each individual load individually. If there is a significant discrepancy between the calculated results and the actual results, it is required to continue the process of elimination until the actual array is identified in order to achieve load recognition.

The real and imaginary components of the fundamental and each harmonic of the normal line current are calculated using the FFT transform, as presented in Table 2. The load is identified using a mix of the formula technique and the exhaustive method. The formula method is initially employed to solve the complex matrix problem and ascertain if the load is singular or not. Furthermore, when dealing with mixed loads, the formula method exhibits a significant rate of misjudgment, particularly when many load combinations are involved. Thus, the initial step is to determine the solution for  $X$ . Next, the calculated result of the derived solution is compared to the actual value. If the comparison does not meet the error percentage of the exhaustive method, the solution for  $X$ , combined with the exhaustive method, is used to determine the specific combination of mixed loads.

#### D. DETECTION RESULTS OF LOAD RECOGNITION

Initially, the loads in Table 1 are computed utilizing the formulaic approach, and the corresponding test outcomes are presented in Table 3. In Table 1, the single loads with load numbers 1 to 5 are represented consecutively by the letters a to e.

In Table 3, the first five working conditions have a load value of 1 in the theoretically calculated matrix, while the other values are 0. This indicates that only one load is connected to the circuit during this time. However, throughout the process of identifying the load, the data collected for sampling is influenced by the voltage of the power grid or other external factors. As a result, there is a certain degree of error when comparing the real sampling data with the ideal data after transformation. This inaccuracy results in the produced results during the solution process typically being imprecise numbers, but rather values that vary within a specific range. Hence, this article permits a margin of error of 25% in the outcomes obtained by the formulaic approach to problem-solving. Specifically, the derived value of  $X$  is permitted to vary between 0.75 and 1.25. Any results exceeding the error are considered invalid values. Table 3 demonstrates that the formula technique has a strong capability in identifying a single load, as the value in the solution  $X$  is nearly equal to 1. Additionally, the method can also recognize two mixed loads when a certain degree of error is permitted. However, when considering three mixed loads, there is a discrepancy between the solution's results and the actual results for comparison. The loads accounted for in the solution only comprise the evaporative cooling fan and the display screen, while excluding the electric fan load. Hence, it is imperative to persist in identifying the three amalgamated loads using the comprehensive approach. If the exhaustive enumeration approach

**TABLE 4.** Exhaustive load identification results.

Load Serial Number	Fundamental		3rd harmonic		5th harmonic		7th harmonic		9th harmonic	
	Real part	imaginary part	Real part	imaginary part	Real part	imaginary part	Real part	imaginary part	Real part	imaginary part
6(calculated value)	0.282044	-0.256812	-0.00164	-0.082468	-0.04678	-0.04274	0.0293928	-0.05118	-0.02803	-0.024608
6(real value)	0.29939	-0.246798	-0.001759	-0.083982	-0.048666	-0.041564	0.0306326	-0.051591	-0.030223	-0.024649
Percentage of error	5.793%	4.057%	6.775%	1.801%	3.874%	2.828%	4.047%	0.797%	7.252%	0.168%
7(calculated value)	0.413501	0.062934	0.0197554	-0.114576	-0.05291	-0.03934	0.0229949	-0.052835	-0.031256	-0.0247
7(real value)	0.408778	0.058905	0.0183463	-0.11454	-0.0565	-0.03782	0.0229416	-0.05327	-0.034861	-0.023425
Percentage of error	1.155%	6.8398%	7.6806%	0.032%	6.364%	3.989%	0.232%	0.816%	10.337%	5.441%
8(calculated value)	0.612391	-0.168296	0.0242352	-0.119285	-0.0431	-0.0443	0.0289872	-0.05313	-0.0273	-0.025291
8(real value)	0.607821	-0.173142	0.024335	-0.116485	-0.047285	-0.040101	0.0297499	-0.056665	-0.026109	-0.02761
Percentage of error	0.752%	2.799%	0.41%	2.403%	8.813%	10.591%	2.563%	6.223%	4.563%	8.398%

is used directly to the three mixed loads listed in Table 1, a minimum of 16 exhaustive enumerations and a maximum of 25 enumerations are required to obtain the accurate outcome. First, calculate the answer for  $X$  using the formula technique. The results of the solution will help define the loads for the evaporative cooling fan and display. Then, use the exhaustive method to identify the loads, which can reduce the number of exhaustive calculations. In this scenario, it requires a maximum of three iterations to obtain the outcome. This work exclusively presents the outcomes of the comprehensive approach utilized for identifying mixed loads, as displayed in Table 4.

The utilization of both formulaic and exhaustive techniques allows for precise recognition of individual and blended loads, hence minimizing the frequency of exhaustive procedures.

## V. EIGENVALUE SELECTION FOR ARC DETECTION

The load's line currents will be measured under both normal and arc fault conditions. Subsequently, the eigenvalues will be retrieved. The eigenvalues that have been obtained are the amplitude of the current fundamental, the total harmonic distortion (THD), the flat shoulder, the time-domain integral value, and the difference-root mean square. Below is an illustration of an eigenvalue analysis conducted on the load of a vacuum cleaner. Figure 3(e)(f) displays the waveforms of the vacuum cleaner during both normal and arc fault situations.

### A. CURRENT FUNDAMENTAL AMPLITUDE

When a series arcing fault arises on a line, it induces a substantial alteration in the current waveform inside the circuit. The fundamental wave is the primary constituent of the current waveform. Hence, the detection of an arcing defect in the circuit can be accomplished by monitoring the alteration in the amplitude of the current's fundamental waveform [33]. The load's fundamental current amplitude is determined by utilizing the Fast Fourier Transform. Figure 9 illustrates that the current fundamental amplitude typically ranges from 1.39 to 1.40 A under normal operating conditions. However,

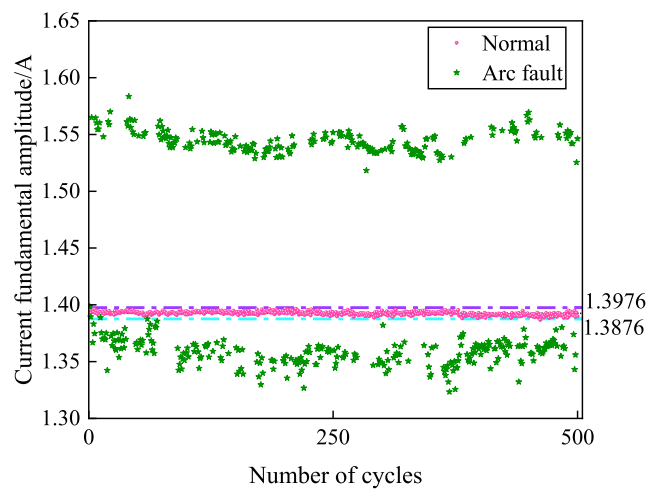


**FIGURE 9.** Plot of current fundamental amplitude for vacuum cleaner load under normal and fault conditions.

in the event of an arc fault in the line, the amplitude of the current fundamental experiences noticeable fluctuations.

### B. TOTAL HARMONIC DISTORTION

The Total Harmonic Distortion is capable of quantifying the proximity of the line current to a sinusoidal waveform. A smaller value indicates a higher proximity to a sine wave. The Total Harmonic Distortion is a measure of the distortion in the line current waveform caused by the occurrence of load arcing faults [33]. In this work, THD is not expressed as a percentage to facilitate calculations. The calculation formula is presented in equation (7).

$$THD = \frac{1}{I_1} \left[ \sum_{i=2}^n (I_i)^2 \right]^{\frac{1}{2}} \quad (7)$$

where  $I_i$  is the  $i$ th harmonic component of the current, and  $I_1$  is the fundamental component of the current. Figure 10 shows that the THD is generally between 0.86 and 0.88 under normal operation, which is basically stable. When arc fault occurs, the arc has randomness, which causes the line current

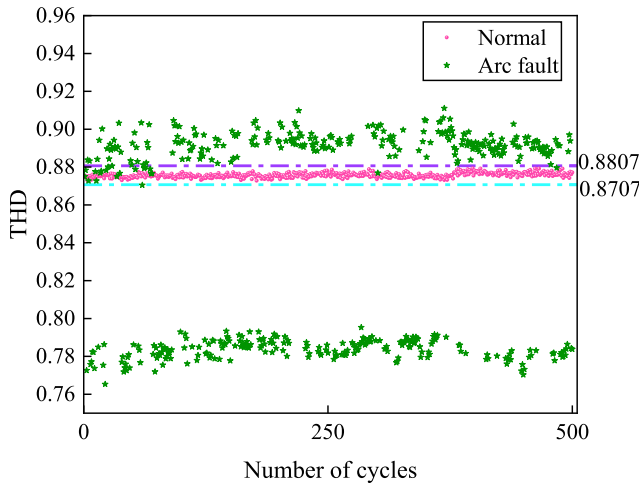


**FIGURE 10.** Plot of total harmonic distortion for vacuum cleaner loads under normal and fault conditions.

waveform to become complex and unstable, thus making the THD change more significant and unstable.

### C. LEVEL SHOULDER

The occurrence of flat shoulder is a significant indication of the load during a fault arc [20]. Equation (8) displays the computation for the flat shoulder.

$$\beta = \frac{\sum_{i=1}^{500} X_i}{500} \quad (8)$$

During each half-cycle, a fixed sampling frequency of 50K is used to collect the current signal of the line. If the absolute value of the current at the sampling point  $X_i$  is below the threshold  $I_{n1}$ , and the absolute value of the difference with the next sampling point is lower than  $I_{n2}$ , then the point  $X_i$  is considered to be the zero crossing of the current. In this case,  $X_i$  is assigned a value of 1; otherwise, it is assigned a value of zero. The flat shoulder value  $\beta$  of the current signal in each half cycle can be determined by tallying the number of zero rest points near the natural zero point. In order to mitigate the influence of interference signals and account for measurement errors, this study chooses a threshold of 0.05A for  $I_{n1}$  and 0.1A for  $I_{n2}$ . It then proceeds to compute the magnitude of the flat shoulder value of the current  $\beta$  for each half-cycle. If the maximum value of the current flowing through the line exceeds 1A, the threshold value for  $I_{n1}$  is set at 0.3A, while the threshold value for  $I_{n2}$  is set at 0.1A. As depicted in Figure 11, the load of the vacuum cleaner during regular operation typically results in a determined flat shoulder value ranging from 0.4 to 0.6. However, when a fault arcing occurs, the majority of cases exhibit a flat shoulder value exceeding 0.6.

### D. TIME DOMAIN INTEGRAL VALUE

During an arc fault, the current waveform of the load will exhibit a plateau or an extended duration shoulder, leading

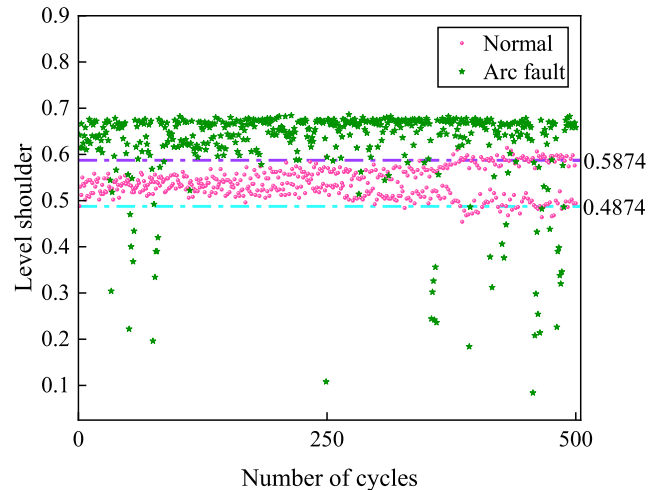


**FIGURE 11.** Flat shoulder plot for normal and faulty vacuum cleaner loads.

to a reduction in the integral value of the current cycle. Thus, the present integral value of the cycle can be retrieved for study [34]. The calculating formula is presented in equation (9),

$$Y_i = \sum_{j=1}^n |X(i)_j| \quad (9)$$

where  $X(i)_j$  is the current value at the  $j$ th sampling point of the  $i$ th cycle and  $n$  is the total number of sampling points in a cycle.

Defects arise from variations in load powers, leading to varying magnitudes of current. This work presents the integral value change coefficient, which quantifies the rate at which the integral value of surrounding cycles changes. The calculation of this coefficient is presented in Equation (10).

$$Y'_i = \frac{Y_{i-1} - Y_i}{Y_{i-1}} \quad (i = 2, 3, \dots) \quad (10)$$

where  $Y_{i-1}$  is the integral value of the previous cycle and  $Y_i$  is the integral value of the current cycle.

Figure 12 displays the coefficient of variation for the integral value of the vacuum cleaner load. During normal situation, the waveform of the load remains relatively stable within each cycle, and the rate of change of the integral value between consecutive cycles approaches zero. When an arc fault happens, the unpredictable nature of the arcing causes a noticeable alteration in the current waveform of the adjacent cycle, leading to a substantial change in the rate of change.

### E. DIFFERENCE-ROOT MEAN SQUARE

During normal load operation, the current waveform exhibits regular periodicity. However, when arcing occurs, the current waveform becomes distorted, displaying irregular phenomena. By extracting the difference-root-mean-square value,

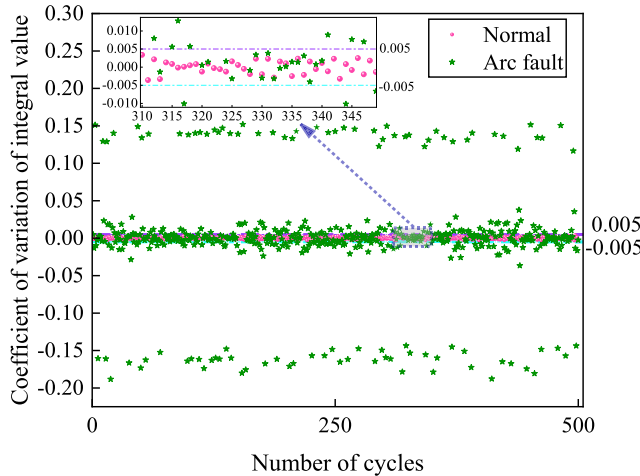


**FIGURE 12.** Plot of the coefficient of variation of the integral of the vacuum cleaner load for normal and fault conditions.

one can determine the presence of a faulty arc [34]. The calculation formula is displayed in equation (11) and equation (12).

$$y(n)_j = X(n)_j - X(n-1)_j \quad (11)$$

In Eq. (11),  $X(n)_j$  is the value at point  $j$  of the  $n$ th cycle and  $X(n-1)_j$  is the value at point  $j$  of the  $(n-1)$ th cycle.

$$Z_n = \sqrt{\frac{\sum_{j=1}^i y(n)_j^2}{i}} \quad (n = 2, 3, \dots) \quad (12)$$

In Eq. (12),  $Z_n$  is the root-mean-square of adjacent cycles, and  $i$  is the total number of sampling points in a cycle.

Additional computations are necessary to address the variations in current intensity among different loads. The root mean square (rms) magnitude is influenced by the level of distortion in the adjacent cycle waveform and the amount of the current. Consequently, the rms value for adjacent cycles under different loads is measured using Equation (13).

$$Z'_n = \frac{1}{a_{n-1}} \sqrt{\frac{\sum_{j=1}^i y(n)_j^2}{i}} \quad (n = 2, 3, \dots) \quad (13)$$

In Eq. (13),  $Z'_n$  is the quantized root-mean-square of adjacent cycles, and  $a_{n-1}$  denotes the current amplitude of the  $(n-1)$ th cycle.

Figure 13 displays the test results of the difference-mean-square of the vacuum cleaner loads. It reveals a notable rise in the difference-mean-square value when arcing occurs, compared to when the loads are functioning correctly.

By analyzing Figures 9–13, numerical alterations in the feature values can be utilized to examine irregularities in the current waveform resulting from the defective arc, thereby achieving the detection and identification of the defective arc. For arc process identification, it is possible to establish a threshold value for the eigenvalue mentioned above. The requirement of the threshold value selected is that as many

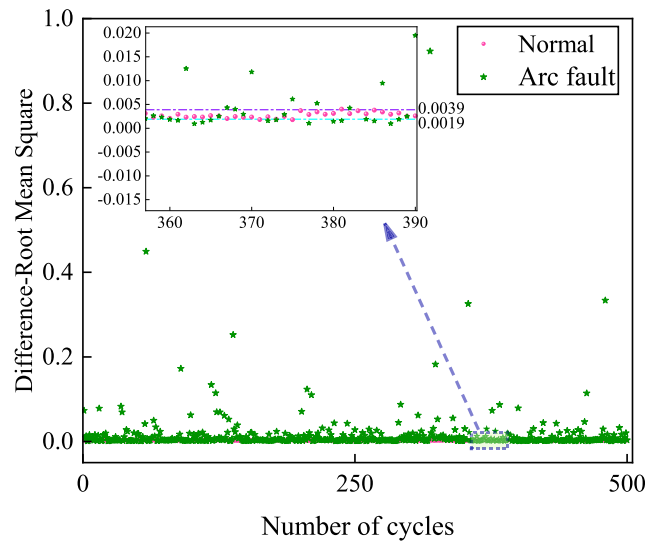


**FIGURE 13.** Root-mean-square plot of the difference between normal and faulty conditions for vacuum cleaner loads.

sample points as possible should be included in the normal situation, while the occurrence of arc fault line current also exists in part of the cycle change is not obvious phenomenon, which will make the eigenvalues during the fault and the eigenvalues of the normal operation in the numerical value of the eigenvalues similar, therefore, it is also necessary to include as few as possible in the range of the threshold value set in the occurrence of arc fault situation of the sample points. Based on the waveform analysis above, it is evident that in order to prevent the impact of minor disturbances caused by the actual load during normal operation on the experimental outcomes, the thresholds for the amplitude of the current fundamental waveform, THD, and time-domain integral value can be established as the average of the eigenvalues during normal situation plus or minus 0.005. The threshold for the Root Mean Square of Difference eigenvalue can be set to the average of the eigenvalues during normal situation plus or minus 0.001. Similarly, the thresholds for the flat-shoulder eigenvalues can be set as the average of the eigenvalues during normal situation plus or minus 0.05. The thresholds are utilized as the criteria for real-time monitoring of the eigenvalues of the feature matrix and the history matrix.

## VI. CHARACTERIZATION MATRIX AND HISTORY MATRIX

The purpose of the feature matrix is to create a database of parameters by gathering the distinctive characteristics of different types of loads. The history matrix is a tool used to document specific attributes of the current over a duration of time when the load is operational [32].

### A. CREATION OF THE FEATURE MATRIX

The feature matrix is constructed using several feature quantities, including the current fundamental amplitude, THD, flat shoulder, time-domain integral value coefficient of variation,

and difference-root-mean-square. These feature quantities are then used to establish thresholds, which are used as the foundation for creating a data feature matrix, as presented in Table 5. The sequence of the order in Table 5 corresponds to the sequential loading order in Table 1.

**TABLE 5. Characteristic matrix.**

Load Serial Number	Current fundamental amplitude ( $\pm 0.05$ )	THD ( $\pm 0.05$ )	Difference - Root Mean Square ( $\pm 0.05$ )	Time domain integral value ( $\pm 0.05$ )	Level shoulder ( $\pm 0.1$ )
1	0.3013	0.0598	0.22886	0.000015	0.105482
2	1.8761	0.0177	0.11688	-0.000009	0.10277
3	1.3971	0.8733	0.00282	0.000113	0.532994
4	0.3414	0.1319	0.1702	-0.000007	0.13867
5	0.6124	0.062	0.1884	0.000014	0.76894
6	0.38199	0.3421	0.2097	0.0000086	0.10128
7	0.414	0.3709	0.1824	-0.000012	0.143524
8	0.6323	0.2472	0.269	-0.000006	0.056462

## B. CREATION OF HISTORICAL MATRIX

The Load Characterization Matrix is a database containing pre-collected eigenvalues. On the other hand, the History Matrix is a record of the present characteristics of the signal across a specific time period. During operation, the circuit is sampled at regular intervals, often every other cycle. The sampling time can be adjusted to meet specific requirements. Subsequently, the eigenvalues are extracted by performing calculations on the sampled data. Once the 7th cycle is surpassed, the real-time sampling data from the 8th cycle will replace the data from the 7th cycle. Similarly, the data from the 7th cycle will replace the data from the 6th cycle, and so on. This process allows for the real-time display of data within the last 7 cycles, ensuring the accuracy of the real-time data. The setting time in this study is 0.5 seconds, which is equivalent to 25 cycles. For the vacuum cleaner load, only the initial 7 cycles of data are shown, as presented in Table 6.

**TABLE 6. History matrix.**

Number of periodic sequences	Current fundamental amplitude	THD	Difference - Root Mean Square	Time domain integral value	Level shoulder
1	1.4373	0.8533	0.0022	0.00016	0.53
2	1.4384	0.8516	0.0024	0.004	0.372
3	1.4338	0.8546	0.0029	-0.0026	0.526
4	1.4378	0.8531	0.0024	0.0021	0.364
5	1.4363	0.8501	0.003	0.0036	0.532
6	1.4676	0.8449	0.0094	-0.0945	0.634
7	1.5887	0.763	0.0021	0.0027	0.638

Based on the provided history matrix, it is evident that there is an eigenvalue that surpasses the threshold during the 6th cycle. At this point, it is imperative to gather numerous cycles using the MLP-SVM model for further analysis.

## VII. ARC FAULT DETECTION RESULT AND ANALYSIS

Once the loads have been recognized, tests are performed on the loads listed in Table 1. A total of 2000 data sets are collected, consisting of 1000 samples taken under normal conditions and 1000 samples taken under fault conditions. This information constitutes a novel dataset. The new dataset categorizes samples under normal conditions as “1” and those with arc fault as “2.” Next, the data set is randomly shuffled and divided into three subsets: 60% is allocated as the training set, 20% as the validation set, and the remaining 20% as the test set. The training set consists of 1200 samples, whereas both the validation and test sets consist of 400 samples each. In this paper, the MLP-SVM model will be trained 20 times to take into account the variability caused by random partitioning of the dataset. By averaging the results of these runs, we may obtain a more reliable estimate of the model’s output. The hyperparameters of the kernel function, Kernel, in the MLP-SVM model are chosen as 0.5, 5, and 50. The hyperparameters of the neurons in each layer of the MLP are chosen as [8], [6,4], and [8,8]. Additionally, the value of  $\theta$  is set to 0.05.

The training results are obtained by training each load by MLP-SVM model as shown in Fig. 14 and Table 7. According to Table 7, Table 8 and Figure 14, the training set achieves an average accuracy of 100% after load recognition. The validation set achieves an average accuracy of 99.947%, and the test set achieves an average accuracy of 99.802%. Meanwhile, the MLP-SVM model also has a good detection effect on loads with inconspicuous current waveform characteristics, such as vacuum cleaners, with a detection accuracy of 99.325%. The output results of the model after load recognition are compared to the results before load recognition, as presented in Table 8 and Table 9. The comparison results indicate that the MLP-SVM model, following load recognition, demonstrates a high level of accuracy in identifying arc fault. The classification results have improved by 1.774% compared to the results obtained before load recognition. And the training time of the model is shortened, the average training time is shortened from 57.4233s before load recognition to 0.2284s, percentage reduction in training time of 99.602%. The MLP-SVM model, after load identification, has a low misjudgment rate on the test set, demonstrates superior learning capability for the training data, possesses high reliability in sample classification, and significantly reduces the model’s running time.

**TABLE 7. Training results for each load after load identification.**

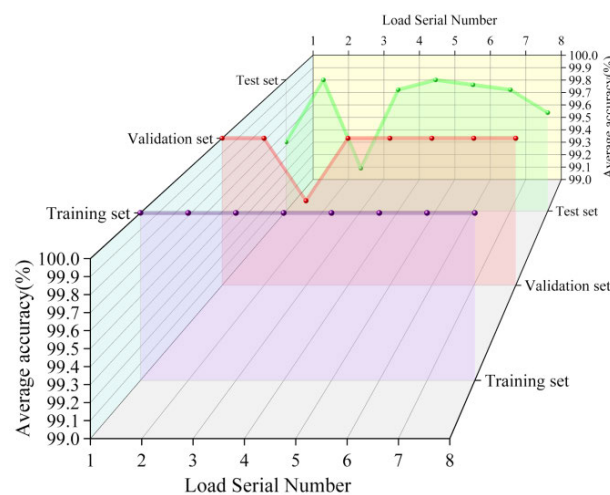
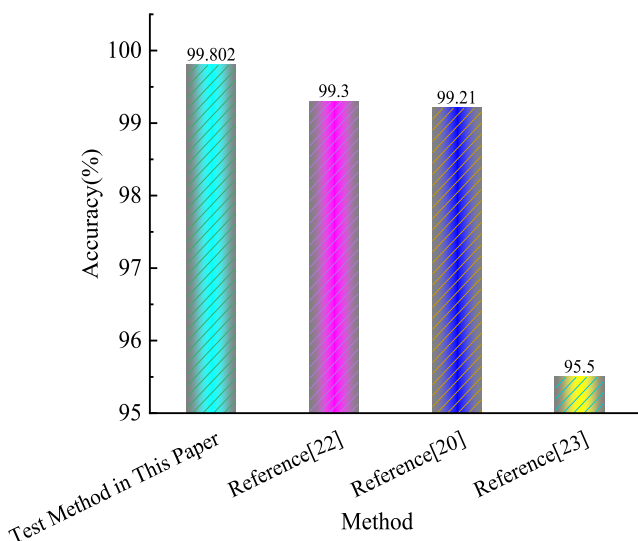
Load Serial Number	Training set	Validation set	Test set
1	100%	100%	99.525%
2	100%	100%	100%
3	100%	99.575	99.325%
4	100%	100%	99.925%
5	100%	100%	100%
6	100%	100%	99.9625%
7	100%	100%	99.925%
8	100%	100%	99.75%

**TABLE 8.** Accuracy comparison before and after load recognition.

Test Method	Training set	Validation set	Test set
MLP-SVM model direct recognition	98.516%	97.986%	98.028%
MLP-SVM model identification after load identification	100%	99.947%	99.802%

**TABLE 9.** Average training time after load recognition.

Test Method	Average training time(s)
MLP-SVM model direct recognition	57.4233s
MLP-SVM model identification after load identification	0.2284s

**FIGURE 14.** Plot of test results for each load after load recognition.**FIGURE 15.** Comparison chart of different test methods.

The findings obtained from the detection method described in this paper are compared with those reported in the literatures [20], [22], and [23]. The comparison is presented in Table 10 and Figure 15. Table 10 and Fig. 15 clearly demonstrate that the average detection accuracy of the method

**TABLE 10.** Comparison of results of different testing methods.

Method	Accuracy
Test Method in This Paper	99.802%
Reference[22]	99.30%
Reference[20]	99.21%
Reference[23]	95.50%

proposed in this paper is 99.802%, surpassing the detection results reported in the literatures [20], [22], and [23]. The load identification method in this paper is more universal, reduces the complexity of subsequent arc fault detection, and improves the accuracy of arc fault detection.

## VIII. CONCLUSION

In this paper, a series arc fault detection method based on the combination of load recognition and MLP-SVM is proposed. To address the issues of series arc fault being easily incorrect ruling and the arc fault characteristics of some loads being insignificant, the line current flowing through the load is first sampled and processed to obtain the eigenvalues. The loads are then identified using a mix of the formula technique and the exhaustive method, and the feature and history matrices for each load are established based on the recognition. Finally, after comparing the data in the feature matrix and history matrix, the MLP-SVM model is employed to detect series arc fault.

1. The experimental results show that after load recognition, the average accuracy of series arc fault detection using MLP-SVM model increases from 98.028% to 99.802%, while training time decreases from 57.4233s to 0.2284s.

2. Furthermore, the MLP-SVM model is employed to overcome the problem of the arc fault properties of specific loads are not significant. The accuracy of the MLP-SVM model for identifying arc fault in loads with negligible current waveform features of series arc fault, such as dust catcher, exceeds 99%.

The method suggested in this research eliminates the effects of complicated loads on arc detection and improves arc fault recognition.

## CONFLICT OF INTEREST STATEMENT

The authors declare no potential conflict of interests.

## REFERENCES

- [1] *Fire Department of Ministry of Public Security, China Fire Yearbook (2004–2010, 2012–2013)*, China Human Resources Press, Beijing, China, 2004.
- [2] *Fire Department of Ministry of Public Security, China Fire Yearbook (2011)*, Int. Culture Publishing Company, Beijing, China, 2011.
- [3] *Fire Department of Ministry of Public Security, China Fire Yearbook (2014–2018)*, Yunnan, China, 2014.
- [4] Y.-X. Luo, Q. Li, L.-R. Jiang, and Y.-H. Zhou, “Analysis of Chinese fire statistics during the period 1997–2017,” *Fire Saf. J.*, vol. 125, Oct. 2021, Art. no. 103400.
- [5] C. Xu, J. X. Sun, J. G. Wang, and Y. Luo, “Study of fault arc protection based on UV pulse method in high voltage switchgear,” *Advanced Materials Research*, vol. 853, no. 853, pp. 641–645, 2013.

- [6] L. Zhao, Y. Zhou, K.-L. Chen, S.-H. Rau, and W.-J. Lee, "High-speed arcing fault detection: Using the light spectrum," *IEEE Ind. Appl. Mag.*, vol. 26, no. 3, pp. 29–36, May 2020.
- [7] C. Vasile and C. Ioana, "Arc fault detection & localization by electromagnetic-acoustic remote sensing," in *Proc. IEEE Radio Antenna Days Indian Ocean*, Oct. 2016, pp. 1–2.
- [8] A. Mukherjee, A. Routray, and A. K. Samanta, "Method for online detection of arcing in low-voltage distribution systems," *IEEE Trans. Power Del.*, vol. 32, no. 3, pp. 1244–1252, Jun. 2017.
- [9] Q. Xiong, S. Ji, L. Zhu, L. Zhong, and Y. Liu, "A novel DC arc fault detection method based on electromagnetic radiation signal," *IEEE Trans. Plasma Sci.*, vol. 45, no. 3, pp. 472–478, Mar. 2017.
- [10] J. Lezama, P. Schweitzer, S. Weber, E. Tisserand, and P. Joyeux, "Arc fault detection based on temporal analysis," in *Proc. IEEE 60th Holm Conf. Electr. Contacts (Holm)*, Oct. 2014, pp. 1–5.
- [11] G. Artale, A. Cataliotti, V. Cosentino, D. Di Cara, S. Nuccio, and G. Tinè, "Arc fault detection method based on CZT low-frequency harmonic current analysis," *IEEE Trans. Instrum. Meas.*, vol. 66, no. 5, pp. 888–896, May 2017.
- [12] Q. Lu, Z. Ye, Y. Zhang, T. Wang, and Z. Gao, "Analysis of the effects of arc volt–ampere characteristics on different loads and detection methods of series arc faults," *Energies*, vol. 12, no. 2, p. 323, Jan. 2019.
- [13] E. Tisserand, J. Lezama, P. Schweitzer, and Y. Berviller, "Series arcing detection by algebraic derivative of the current," *Electr. Power Syst. Res.*, vol. 119, pp. 91–99, Feb. 2015.
- [14] J. Hui and J. Yuan, "Neural network-based adaptive fault-tolerant control for load following of a MHTGR with prescribed performance and CRDM faults," *Energy*, vol. 257, Oct. 2022, Art. no. 124663.
- [15] J. Hui, Y.-K. Lee, and J. Yuan, "Adaptive active fault-tolerant dynamic surface load following controller for a modular high-temperature gas-cooled reactor," *Appl. Thermal Eng.*, vol. 230, Jul. 2023, Art. no. 120727.
- [16] J. Hui, Y.-K. Lee, and J. Yuan, "Load following control of a PWR with load-dependent parameters and perturbations via fixed-time fractional-order sliding mode and disturbance observer techniques," *Renew. Sustain. Energy Rev.*, vol. 184, Sep. 2023, Art. no. 113550.
- [17] J. Hui and J. Yuan, "Chattering-free higher order sliding mode controller with a high-gain observer for the load following of a pressurized water reactor," *Energy*, vol. 223, May 2021, Art. no. 120066.
- [18] J. Li, G. Zou, W. Wang, N. Shao, B. Han, and L. Wei, "Low-voltage series arc fault detection based on ECMC and VB-SCN," *Electric Power Syst. Res.*, vol. 218, May 2023, Art. no. 109222.
- [19] Q. Lu, T. Wang, B. He, T. Ru, and D. Chen, "A new series arc fault identification method based on wavelet transform," in *Proc. 43rd Annu. Conf. IEEE Ind. Electron. Soc.*, Beijing, China, Oct. 2017, pp. 4817–4822.
- [20] X. Han, D. Li, L. Huang, H. Huang, J. Yang, Y. Zhang, X. Wu, and Q. Lu, "Series arc fault detection method based on category recognition and artificial neural network," *Electronics*, vol. 9, no. 9, p. 1367, Aug. 2020.
- [21] Q. Gong, Q. Gao, X. Qu, K. Peng, L. Feng, and C. Xiao, "Low-voltage AC series arc fault location method based on RBF neural network," *Electr. Power Syst. Res.*, vol. 229, Apr. 2024, Art. no. 110176.
- [22] J. Jiang, Z. Wen, M. Zhao, Y. Bie, C. Li, M. Tan, and C. Zhang, "Series arc detection and complex load recognition based on principal component analysis and support vector machine," *IEEE Access*, vol. 7, pp. 47221–47229, 2019.
- [23] N. Qu, J. Zuo, J. Chen, and Z. Li, "Series arc fault detection of indoor power distribution system based on LVQ-NN and PSO-SVM," *IEEE Access*, vol. 7, pp. 184020–184028, 2019.
- [24] *Arc-Fault Circuit-Interrupts*, document UL1699, 1999.
- [25] National Fire Protection Standardization Technical Committee Fire Detection and Alarm Sub-Technical Committee, document GB14287.4-2014, 2014.
- [26] National Technical Committee for Standardization of Low-voltage Electrical Appliances., document GB/T31143-2014, 2014.
- [27] T. Yu, X. Li, Y. Cai, M. Sun, and P. Li, "S2-MLP: Spatial-shift MLP architecture for vision," in *Proc. IEEE/CVF Winter Conf. Appl. Comput. Vis. (WACV)*, Waikoloa, HI, USA, Jan. 2022, pp. 3615–3624.
- [28] R. Lin, Z. Zhou, S. You, R. Rao, and C.-C. J. Kuo, "Geometrical interpretation and design of multilayer perceptrons," *IEEE Trans. Neural Netw. Learn. Syst.*, pp. 1–15, Feb. 2022.
- [29] N. Innan, M. A. Z. Khan, B. Panda, and M. Bennai, "Enhancing quantum support vector machines through variational kernel training," *Quantum Inf. Process.*, vol. 22, no. 10, p. 374, Oct. 2023.
- [30] S. Saha, A. Saha, T. K. Hembram, B. Kundu, and R. Sarkar, "Novel ensemble of deep learning neural network and support vector machine for landslide susceptibility mapping in Tehri region, Garhwal Himalaya," *Geocarto Int.*, vol. 37, no. 27, pp. 17018–17043, Dec. 2022.
- [31] Y.-B. Zhang, P.-Y. Xu, J. Liu, J.-X. He, H.-T. Yang, Y. Zeng, Y.-Y. He, and C.-F. Yang, "Comparison of LR, 5-CV SVM, GA SVM, and PSO SVM for landslide susceptibility assessment in Tibetan Plateau area, China," *J. Mountain Sci.*, vol. 20, no. 4, pp. 979–995, Apr. 2023.
- [32] L. W. Zhang, *Research on Correlation Algorithm for Power Load Pattern Recognition*. Shijiazhuang, China: Shijiazhuang Railway University, 2013.
- [33] Z. Dongsong, *Research on Load Identification Technology Based on SVM*. Chengdu, China: Hangzhou University of Electronic Science and Technology, 2017.
- [34] D. Aihua, K. Linjuan, and D. Jingjing, "Fault arc detection method based on mutation theory information fusion," *J. Power Syst. Automat.*, vol. 28, no. 5, pp. 35–40, 2016.



**NENGQI WU** was born in Loudi, Hunan, China. He received the B.Eng. degree from Hebei University of Engineering, in 2023. He is currently pursuing the master's degree in electrical engineering with China University of Mining and Technology, Beijing. His major is electrical engineering and automation. His research interest includes ac series fault arc detection.



**MINGYI PENG** was born in Yichun, Jiangxi, China. He received the B.Eng. degree in electrical engineering and automation from Chongqing Jiaotong University, Chongqing, China, in 2023. He is currently pursuing the M.Eng. degree in electrical engineering with China University of Mining and Technology, Beijing. His research interests include applications in arc detection for ac and dc faults.



**JIAJU WANG** received the B.Eng. degree in electrical engineering from Northwest Minzu University, in 2021. He is currently pursuing the M.S. degree in electrical engineering with the School of Mechanical and Electrical Engineering, China University of Mining and Technology, Beijing. His research interests include power system protection and control.



**HONGLEI WANG** received the bachelor's degree from Henan Institute of Science and Technology, in 2020. He is currently pursuing the master's degree in electrical engineering with China University of Mining and Technology, Beijing. His research interests include coal mine electrical safety, intelligent power supply and distribution, and fault arc detection technology.



**QIWEI LU** received the B.S. degree in electrical engineering from Heilongjiang University of Science and Technology, Harbin, China, in 1997, and the M.S. and Ph.D. degrees from China University of Mining and Technology, Beijing, China, in 2002 and 2006, respectively. From 2013 to 2014, he was a Visiting Scholar with the Future Renewable Electric Energy Delivery and Management (FREEDM) Systems Center, North Carolina State University, Raleigh, NC, USA. He is currently a Professor with the School of Mechanical Electronic and Information Engineering, China University of Mining and Technology. His research interests include dc distribution systems, fault detection, locomotive regenerative braking energy recovery, and electrical safety.



**MINGZHE WU** (Member, IEEE) received the B.Sc. degree in electrical engineering from China University of Mining and Technology, Beijing, China, in 2019, and the Ph.D. degree from the University of Alberta, Canada, in 2023. From 2017 to 2019, he was a Research Assistant with the Department of Electrical Engineering, Tsinghua University, China, involved in power system resilience and multilevel converters. He is currently a Lecturer with the Department of Electrical Engineering, China University of Mining and Technology. His current research interests include topology, modulation, and control of high-power converters.



**HANNING ZHANG** was admitted to China University of Mining and Technology, Beijing, in 2022. He is currently pursuing the bachelor's degree in electrical engineering and automation. His main research interests include power electronics and power transmission technology.



**FANFAN NI** is currently pursuing the bachelor's degree in electrical engineering with China University of Mining and Technology, Beijing. His research interests include coal mine electrical safety, intelligent power supply and distribution, and fault arc detection technology.

• • •